Galvanic-submerged photo synthesis of crystallites: Fabrication of ZnO nanorods@ Cu-surface

Yuki Takahashi†, Kento Hiraiwa†, Melbert Jeem‡, Lihua Zhang‡, and Seiichi Watanabe*‡

†Graduate School of Engineering and ‡Faculty of Engineering, Hokkaido University, N13, W8, Kita-ku, Sapporo, Hokkaido 0608628, Japan

Corresponding author at Faculty of Engineering, Hokkaido University, N13, W8, Kita-ku, Sapporo, Hokkaido, 060-8628, Japan.

Email address: sw004@eng.hokudai.ac.jp (S. Watanabe)

Abstract

In this study, we report a facile fabrication method of 1-D ZnO nanorods (NRs) on a copper substrate surface by means of galvanic contact reactions. Instead of using bimetallic aqueous solution for the galvanic reactions, UV illumination on the Zn contacted with Cu surface in pure water environment was implemented, leading to galvanic combined submerged photo-synthesis of crystallites (G-SPSC) process. A pencil-like and flat-tip shape of NRs growth can be controlled as a function of UV irradiation time. In order to grow fine NRs, the galvanic process was essential for Zn^{2+} and OH^- ions production. In particular, OH^- accumulated at the vicinity surface of Cu to achieve a locally alkaline environment. Then, UV irradiation assisted the ZnO NRs initiated by water splitting process. Oxygen vacancy (V_O) was responsible for the growth of pencil-like shape NRs. A blue shift in visible light region of photoluminescence (PL) spectra was observed when the pencil-like NRs transformed into flat-tip shape. The successful *p-n* junction between Zn-Cu also was observed in their PL spectra, which dictated by the formation of zinc antisite (Zn_O). The G-SPSC method approach is versatile for other bimetallic system adaptation and is promising for large-scale environmentally friendly synthesis of opto-electronic devices.

1. Introduction

The multifunctional characteristic of nanosized semiconductor can be dependent on its morphology control, which is driven by their bandgap alteration caused by the crystal lattice defects. The study on nanostructure semiconductor has thus inherently attracted many researchers for the exploration of opto-electronic devices [1,2], ranging from lasers [3,4], to light-emitting diodes [5] to many types of transistors [6]. Metal oxides materials: silicon dioxide (SiO_2), tin dioxide (SnO_2), copper oxide (CuO, Cu_2O), zinc oxide (ZnO), etc. captured the attention owing to their inexpensive, non-toxic, chemical stability properties, as well as abundantly available on earth. In particular, ZnO, an *n*-type semiconductor is easily recognizable in pharmaceuticals, batteries [7], catalysts [8,9], resins, and LED applications [10] on account of its wide bandgap energy (Eg = 3.37 eV) and high exciton binding energy of ~60 meV.

Furthermore, the incorporation of *p*-type semiconductor to *n*-type ZnO has enable its heterostructure nanofabrication, beneficial for multifunctional properties on photovoltaic devices [11,12]. This is because the bandgap alignment can be freely altered; favored by its nanoscale size, adhering to the electrons transfer due to quantum size effect. The behavior of the hetero-nanostructures is then depending on the local atomic arrangement at the junction. Conventionally, this arrangement can be carefully adjusted by means of hydrothermal methods, which includes the setting parameters of electrolytes composition, temperatures, applied voltage, and substrates employed. However, the method parameters always have drawbacks on the materials finishing, particularly after involvement of impurity effect, high temperature requirement, and its impact to the environment.

For this concern, the current study demonstrates a facile method to fabricate one-dimensional heterostructures ZnO nanorods (NRs) on a Cu (ZnO@Cu) substrate surface by means of galvanic contact reaction. The galvanic contact reaction is performed on the basis of our previous experiment approach, using submerged photosynthesis of crystallites (SPSC) [13-15]. SPSC method only utilizes pure water and light irradiation ranging from UV ($\lambda = 365$ nm) to visible light under ambient condition to fabricate various metal oxide nanostructures. Using this environmental benign approach, galvanic combined SPSC (G-SPSC) method was implemented to study the ZnO@Cu NRs growth mechanism, beneficial for the fundamental understanding of G-SPSC. In addition, we also presented the optical properties of the fabricated ZnO@Cu NRs to highlight G-SPSC future application in opto-electrical devices manufacturing.

2. Experimental

2.1 G-SPSC experiment

The G-SPSC experiments setup includes metal plates (20 mm × 5 mm × 0.5 mm) and wires (φ: 0.5 mm, 99.99%) of Zn and Cu (Nilaco, Tokyo, Japan) with purity of 99.5%, 99.96%, purified water (Trusco, pH 6.5~7.0, resistivity 0.17μS/cm), and UV ($\lambda = 365$ nm) light (UVP, B-100AP, USA). The Zn and Cu plates were ultrasonically cleaned in ultrapure water for 5 minutes prior G-SPSC experiment. After cleansing, for the purpose of galvanic contact, the Zn surface contact with Cu were adjusted by wire binding of Zn wire to Cu or Cu wire binding of Zn to Cu plate (Fig. 1a). For G-SPSC experiment, the binded Zn-Cu plates were immersed in deaerated purified water and irradiated under UV light for 24 ~ 48 hours (Fig. 1b) inside a dark chamber to obtain ZnO@Cu NRs (Fig. 1c). The effective UV intensity toward the samples was 20 mW/cm^2.

2.2 Physical and chemical characterization

After G-SPSC, the surface morphology was observed using field emission type scanning electron microscopy (FE-SEM, JEOL, JSM-7001FA). Transmission electron microscopy (TEM), selected area electron diffraction (SAED) pattern and high-resolution TEM (HRTEM) images were obtained by FEI

Titan Cubed operated at 300 kV. The NRs growth orientation was examined by X-ray diffraction (XRD) (Rigaku, Miniflex) equipped with Cu Kα radiation (λ = 1.5406 Å). Analysis of chemical properties was performed with SEM-energy dispersive X-ray spectroscopy (EDX). X-ray photoelectron spectroscopy (XPS, JEOL, JPS-9200) measurement was conducted with Al-Kα X-ray source (1486.6 eV). The obtained XPS spectra were analyzed using SpecSurf (analysis) software. Savitzky-Golay method was performed to substract the background. All spectra were calibrated to the C 1*s* electron peak at 285.1 eV. Then, the peak positions and areas were optimized by weighted least-square fitting method using 70% Gaussian and 30% Lorentzian line profile shapes.

2.3 pH change investigation and optical properties study

The water pH fluctuation was observed due to electron transfer occurred by the galvanic contact. pH measurement was done by using pH meter (Horiba, LAQUA, F-74) containing Ag/AgCl electrode (Horiba, LAQUA, PURE IL 9600-10D). Qualitative pH change was administered by using bromothymol blue (BTB) solution ($C_{24}H_{28}Br_2O_5S$, molar mass = 0.04W/V%, SHOWA, 6.25%). A BTB agar solution was prepared by boiling 10 ml of BTB solution mixed with 5 g of agar (Hayashi Pure Chemical Ind., Ltd.) and 300 ml purified water at 100 ℃ (Fig. 6a). Here, BTB solution color will turn from green to blue to denote alkaline pH (7.6~) level (Fig. 6b). Then, G-SPSC experiment was conducted on the binded Zn-Cu plates immersed inside the BTB agar solution. Color change of the BTB agar solution was observed (Fig. 6c). For the optical properties investigation, room-temperature photoluminescence (PL) spectra were collected under excitation by a 325 nm He Cd continuous-wave laser operated at its maximum output of 16 mW. The PL spectra were recorded using an Acton SP2150 imaging spectrograph (Princeton Instruments) with a nominal resolution of 0.4 nm. Spectra peak deconvolution was implemented by Gaussian function.

3. Results and discussion

3.1 Surface morphology analysis

One-dimensional ZnO NRs were effectively grown on the Cu surface after G-SPSC at ambient condition (Fig. 2b-c). The homogeneous NRs hexagonal facets with diameter of 200 nm and ~1 μm in length also translates its uninterrupted growth as no dendritic or nanoflowers structures were observed. Normally, those structures would appear when there is high supersaturation and deposition rate of oxide layer on the metallic surface. And in order to ensure uninterrupted ZnO NRs formation, supply of H^+ or OH^- is controlled by the molarity of the acidic/alkaline solution. On the contrary, G-SPSC treatment only utilized neutral water. The resultant grown NRs are in good crystallinity based on its XRD spectrum (Fig. 2d). Main observed ZnO peak in the XRD spectrum correspond to (100), (002), (101) at 31.10°, 33.74°, and 35.56°, respectively of the ZnO hexagonal wurtzite crystal structure (JCPDS 79-0208) [13,16,17]. The strongest (111) peak at 42.66° (JCPDS 71-4611) is originated from

the Cu plate. The NRs have their highest XRD peak along the (002) plane, marking its preferred growth orientation along the plane of hexagonal {*P*63*mc*(186)} phase.

The detailed NRs crystal structure was further characterized by TEM and HRTEM (Fig. 3). Fig. 3a shows a pencil-like ZnO NR grown with 200 nm diameter. Its SAED pattern (Fig. 3b) revealed its single crystallinity characteristic. Moreover, consistent with the XRD result, HRTEM image show the NRs excellent crystallinity along the <001> direction (Fig. 3c-d). In Fig. 3d, a clear lattice fringe proved that the NR is singly crystalline along its growth *c*-axis growth direction. From HRTEM image, the spacing of the adjacent lattice fringe along the (002) plane is 0.26 nm.

On the basis of SEM-EDX result, oxygen deficiency was confirmed on the ZnO@Cu NRs, especially when the NRs are in pencil-like shape. This result was also found in previous study [16], which also point up the NRs growth controllability as the function of UV irradiation time. Pencil-like NRs was observed after UV 24h irradiation and longer irradiation until 48h resulted in flat-tip NRs formation. The function of UV light towards the NRs growth behavior was clearly seen based on UV light presence or absence experiment. Very less NRs growth was observed on Cu surface with absence of UV irradiation compare with UV irradiated sample (Fig. S1a-b). However, galvanic effect was still observed on the Zn wire surface although Zn sacrifice reaction was not coarsely achieved. $Zn(OH)_2$ was dominant over small ZnO particles.

Concerning oxygen species other than ZnO, i.e., $Zn(OH)_2$ in the sample, the NRs surface composition was investigated by XPS analysis. In Fig. 4a, the wide scan survey spectrum indicated strong presence of zinc (Zn) and oxygen (O) species. Copper (Cu) peak from the Cu plate accompany in the spectrum, as well as carbon (C) [18,19]. The C peak was due to atmospheric contamination. High resolution scan of Zn 2*p*1/2 and Zn 2*p*3/2 at 1044.53 eV and 1021.53 eV, respectively confirm that Zn element was in the form on Zn^{2+} chemical state on the ZnO@Cu surface [20]. The O 1*s* peak has a high intensity on the sample surface. It stems from the ZnO NRs and will asymmetrically appear when there is more than one type of oxygen species from the NRs surface. Peak deconvolution was performed on O 1*s* spectra of UV 24h and UV 48h irradiated samples (Fig. 4c-d). Peak deconvolution result (Table 1) showed prominent peaks at 530.1-530.3 eV related with the oxygen lattice of ZnO [21,22]. $Zn(OH)_2$ peak can be apprised by the shoulder on the spectrum, which can be assigned on 531.3 eV and 531.6 eV on UV 24h and UV 48h sample, respectively. Generally, these peaks are associated with oxygen vacancy, which OH^- group tends to be adsorbed on the surface, resulting in $Zn(OH)_2$ production. In conjuncture of surface adsorption, a loosely bound oxygen will also be created, which can assigned to 532.0 – 532.3 eV peaks. The UV 48h sample (Fig. 4d) has higher content of $Zn(OH)_2$, given that its shoulder is more appearing than that of in UV 24h sample. However, XPS quantitative analysis indicated that the latter has less oxygen. Zn:O ratio of UV 24h and UV 48h are 51.6:48.4 and 45.2:54.8, respectively. In this case, $Zn(OH)_2$ increased with longer UV irradiation, but not necessarily affected in increasing oxygen defects in the NRs. $Zn(OH)_2$ in UV 48h sample is thus

particularly occurred on the Cu plate surface as a consequence of local OH^- accumulation on the Cu surface. This suggestion will be further elaborated in the G-SPSC mechanism section, as well as in the photoluminescence (PL) analysis result.

The G-SPSC experiment highlights the function of light, water pH, and galvanic contact reaction toward formation of ZnO@Cu NRs. In this concern, the UV light irradiation increased the water temperature to ~45°C and the temperature was consistent until UV 24h/ 48h irradiation to yield overall water pH of 7.5. From here, the 1-D NRs growth was attributed by the consistent temperature and uniform deposition of metal oxide in locally alkaline environment. This observation is consistent with the uniform blue color transformation on the BTB agar solution (Fig. 6c), which will also be discussed later. More importantly, the galvanic reaction was necessary, as a comparison result of non-galvanic with galvanic contacted Zn-Cu plates shows clear ZnO@Cu NRs formation on the latter (Fig. 2e-f).

3.2 The mechanism of G-SPSC

Fig. 5 illustrates the ZnO@Cu NRs growth mechanism under G-SPSC. Three responsible reactions are considered toward combining the galvanic-photochemical processes. Firstly, galvanic reaction is established by contact surface of Zn-Cu plate according to the following reaction:

$$\text{Anodic: } Zn \rightarrow Zn^{2+} + 2e^- \quad (1)$$

$$\text{Cathodic: } H_2O + e^- \rightarrow OH^- + H_{ad} \text{ or } H_2O + 1/2\,O_2 + 2e^- \rightarrow 2OH^- \quad (2)$$

The standard reduction potential (SRP) of Zn metal is E^0 (Zn^{2+}/Zn) = -0.76 V *vs.* standard hydrogen electrode (SHE) and the SRP value of Cu metal is E^0 (Cu^{2+}/Cu) = 0.34 V *vs.* SHE. The SRP values imply that Cu can be easily deposited on Zn metal through oxidation of Zn, setting Zn as anode and Cu as the cathode. However, since the solution contain only water; absence of Cu^{2+} ions, galvanic corrosion reaction is promoted between the two metals, i.e., Zn metal loses electrons [23] and migrates to the water (eq. 1). As the SRP value of (O_2/OH^-) system is 0.40 V *vs.* SHE, cathodic reaction of water with released electron, as well as consumption of dissolved oxygen to generate OH^- also arise (eq. 2). These reactions took place at the vicinity surface of Cu, attracting OH^- accumulation on the Cu surface. Consequently, Cu surface becomes locally alkaline [24,25] and promote the second reaction, which is the formation of ZnO NRs precusors:

$$Zn^{2+} + 2OH^- \rightarrow Zn(OH)_2 \quad (3)$$

$$Zn(OH)_2 + 2OH^- \rightarrow [Zn(OH)_4]^{2-} \quad (4)$$

$$[Zn(OH)_4]^{2-} \rightarrow ZnO + 2OH^- + H_2O \quad (5)$$

Zn^{2+} ions and OH^- from equations 1-2 formed into zinc hydroxide ($Zn(OH)_2$) (eq. 3). Further,

$Zn(OH)_2$ will react with OH^- to form $[Zn(OH)_4]^{2-}$. The formation of $Zn(OH)_2$ and $[Zn(OH)_4]^{2-}$ is spontaneous to form an insulation layer [26]. Due to this layer, only small amount of ZnO was formed through dehydration of $[Zn(OH)_4]^{2-}$, thus creating only ZnO nanoparticles. In order to permit ZnO NRs growth, UV light was essential to give in the third reaction, which is the photochemical enhancement of local alkaline region [13].

$$ZnO + h\nu \rightarrow ZnO(e^- + h^+) \quad (6)$$

$$H_2O + h^+ \rightarrow \bullet OH + H^+ \quad (7)$$

$$\bullet OH + e^-_{aq} \rightarrow OH^- \quad (8)$$

Pair of free electrons and holes were firstly created via bandgap excitation (3.37 eV < E_{pH}) (eq. 6). Then, water splitting reaction took place to generate OH radical (•OH) and H^+ ions. In water radiolysis, micro-second-order formation of transient species (H, •OH, e^-_{aq}) [27,28] will transform the •OH to OH^- (eq. 8). In this case, through hydration of the free electron ($e^- \rightarrow e^-_{aq}$) [13]. In particular, the increase of OH^- occur at the tip of the ZnO nanoparticles, caused by separation of e^- and h^+ pair, where e^- is rich at the tip area. This prevailing reaction was observed by Jeem et al. [16], which high energy absorption at a tip-edge of a NR creates an opto-electrical hotspot allowing the photochemical reactions above. And the observed phenomena occur because of oxygen vacancy existence on the precursor lattice. Subsequently, dehydration of $[Zn(OH)_4]^{2-}$ (eq. 5) is accelerated and nucleate on the positively charge {0001} facet, resulting in vertical growth of ZnO. Nevertheless, the effective UV light function will not be realized if not accompanied by the increase of water temperature, which creates a large driving force for the nucleation as well, although not dominant to facilitate the overall growth of ZnO@Cu NRs (Fig. S1).

3.3 Galvanic contact study via BTB agar solution

Although the SRP values of Zn (-0.76 V) and Cu (0.34 V) are well known in general galvanic cell setup, it is still not possible to obtain the real SRP value especially in the water system without using SHE. In an effort to confirm the galvanic contact reactions (eq. 1-2), empirical study was implemented by qualitative pH change observation of BTB agar solution (Fig. 6). The initial green color of BTB solution will turn into yellow and blue in the presence of acidic and alkaline substance, respectively (Fig. 6b). The yellowish color of BTB agar in Fig. 6c is solely due to heating and mixing with agar, disregarding the acidic substance presence. Without UV irradiation, the galvanic contact observation was carried on for Zn-Cu plates at room temperature. Interestingly, the BTB color changed to blue at entire margin of Cu plate (Fig. 6c, 5min). And the color change gradually evolves while maintaining to envelop the Cu plate with uniformity. This translates to gradual and uniform OH^- distribution near the Cu surface to let the 1-D ZnO NRs formation during G-SPSC. In addition, the pH value at 24h was 10.43.

3.4 Photoluminescence result

Comparing 24h and 48h UV irradiated ZnO@Cu samples, room temperature PL result shows a blue-shift occurrence (638 nm → 513 nm) in their visible light region. No shift in the 380 nm near band edge (NBE) emission [29]. However, the NBE emission in UV 24h NRs was more suppressed compare to the UV 48h NRs. This is due to dominance of oxygen vacancy (V_O) in the UV 24h NRs, as also shown in XPS quantitative analysis. The V_O acted as nonradiative centers for the recombination of photoexcited electron-hole pair [30,31]. Less density of V_O will allow more radiative electron-hole pairs recombination between conduction band (CB) and valence band (VB) to give rise higher intensity of UV emission, as exhibited by the UV 48h NRs. Thus, the 638 nm peak can be attributed to V_O. 513 nm peak in UV 48h NRs is derived by oxygen antisite (O_{Zn}) [16,32]. Here, zinc replacement by oxygen can be stated by the Zn:O ratio from XPS result on UV 48h NRs. Moreover, an appearing shoulder on 570 nm peak in UV 48h NRs was observed, presumably originated from the $Zn(OH)_2$ film [33] on Cu surface.

Now, considering the broad visible light region in both samples, most of the nonradiative recombination processes may occur on the NRs surface. Those processes can be expressed by the tendency of ZnO to adsorb negative charge species when V_O is present [34,35], making the surface became negatively charged. The negative charges will be desorbed by photoexcited holes during PL and created a band bending at the interface of ZnO-Cu. As a consequence, a p-n junction between ZnO and Cu is established, resulting the 700-710 nm peaks (Fig. 7a-b, Table 2). An interaction between intrinsic defects in ZnO will drive the formation of zinc antisite (Zn_O) for the 700-710 nm peaks. A detailed band bending mechanism is discussed in Hiraiwa et al. report, which highlights the applicability of G-SPSC towards other metals.

3.5 Conclusion

In this study, 1-D ZnO NRs were successfully fabricated on a Cu plate surface by initiating a galvanic contact reaction between Zn@Cu surface in a submerged photo-synthesis of crystallites (SPSC) process. The galvanic process was essential for Zn^{2+} and OH^- ions production. Due to ionization potential difference between Zn and Cu, OH^- ions accumulated at the vicinity of Cu surface to make it as locally alkaline environment. UV illumination toward the galvanically contacted Zn@Cu sample in pure water assisted the ZnO NRs growth, which also demonstrated the controllability of pencil-like shape and flat-tip NRs fabrication under 24h and 48h irradiation, respectively. Supported by EDX and XPS analysis, oxygen vacancy (V_O) in ZnO was found responsible for the pencil-like shape NRs growth as well as a driving force for water splitting process in participating photochemical reactions. A blue-shift in visible light region of PL spectra was observed when the pencil-like shape transformed to flat-tip NRs. This is due to continuous deposition of OH^- on the NRs surface,

subsequently transforming V_O defects in pencil-like shape NRs to oxygen antisite (O_{Zn}) on the flat-tip NRs surface. A p-n junction established at the interface of Zn-Cu reflected a low energy formation near 700 nm in the PL spectra. The energy is originated from zinc antisite (Zn_O). The G-SPSC process has highlighted an environmentally friendly method in fabricating nanostructure materials. In related work, Hiraiwa et al. reports the G-SPSC application toward Zn substrates combined with noble metals (Au, Pt, Ag, Ag, Cu) as well as W and Ni metals for futuristic feasible large-scale luminescent device technology.

Acknowledgement

This work was financially supported by the “Nanotechnology Platform” from the Ministry of Education, Culture, Sports, Science and Technology (MEXT). All authors contributed equally to this work and declare no competing financial interest.

References

[1] A.B. Djurišić, A.M.C. Ng, X.Y. Chen, ZnO nanostructures for optoelectronics: Material properties and device applications, Progress in Quantum Electronics, 34 (2010) 191-259.

[2] C. Li, X. Li, D. Wang, Fabrication of ZnO Thin Film and Nanostructures for Optoelectronic Device Applications, in: P. Mele, T. Endo, S. Arisawa, C. Li, T. Tsuchiya (Eds.) Oxide Thin Films, Multilayers, and Nanocomposites, Springer International Publishing, Cham, 2015, pp. 239-271.

[3] D. Vanmaekelbergh, L.K. van Vugt, ZnO nanowire lasers, Nanoscale, 3 (2011) 2783-2800.

[4] S. Wu, S. Buckley, J.R. Schaibley, L. Feng, J. Yan, D.G. Mandrus, F. Hatami, W. Yao, J. Vučković, A. Majumdar, X. Xu, Monolayer semiconductor nanocavity lasers with ultralow thresholds, Nature, 520 (2015) 69.

[5] J.-T. Chen, W.-C. Lai, Y.-C. Chang, J.-K. Sheu, W.-C. Sen, GaN-based light emitting diodes with micro- and nano-patterned structures by femtosecond laser nonlinear decomposition, 2012.

[6] R. Ahmad, M.-S. Ahn, Y.-B. Hahn, ZnO nanorods array based field-effect transistor biosensor for phosphate detection, J. Colloid Interface Sci., 498 (2017) 292-297.

[7] M. Ahmad, S. Yingying, H. Sun, W. Shen, J. Zhu, SnO2/ZnO composite structure for the lithium-ion battery electrode, Journal of Solid State Chemistry, 196 (2012) 326-331.

[8] H. Lorenz, M. Friedrich, M. Armbrüster, B. Klötzer, S. Penner, ZnO is a CO2-selective steam reforming catalyst, Journal of Catalysis, 297 (2013) 151-154.

[9] Y. H M Lu, L. X Xu, C. L Xu, Q. Zhang, X. N Zhang, S. Xu, M. Xu, K. Ostrikov, Enhanced ultraviolet photocatalytic activity of Ag/ZnO nanoparticles synthesized by modified polymer-network gel method, 2015.

[10] D.C. Kim, W.S. Han, B.H. Kong, H.K. Cho, C.H. Hong, Fabrication of the hybrid ZnO LED structure grown on p-type GaN by metal organic chemical vapor deposition, Physica B: Condensed Matter, 401-402 (2007) 386-390.

[11] X.-M. Song, C. Yuan, Y. Wang, B. Wang, H. Mao, S. Wu, Y. Zhang, ZnO/CuO photoelectrode with n-p heterogeneous structure for photoelectrocatalytic oxidation of formaldehyde, Applied Surface Science, 455 (2018) 181-186.

[12] A. Kargar, Y. Jing, S.J. Kim, C.T. Riley, X.Q. Pan, D.L. Wang, ZnO/CuO Heterojunction Branched Nanowires for Photoelectrochemical Hydrogen Generation, Acs Nano, 7 (2013) 11112-11120.

[13] M. Jeem, M.R.M. bin Julaihi, J. Ishioka, S. Yatsu, K. Okamoto, T. Shibayama, T. Iwasaki, T. Kato, S. Watanabe, A pathway of nanocrystallite fabrication by photo-assisted growth in pure water, Scientific

Reports, 5 (2015) 11429.
[14] L. Zhang, M. Jeem, K. Okamoto, S. Watanabe, Photochemistry and the role of light during the submerged photosynthesis of zinc oxide nanorods, Scientific Reports, 8 (2018) 177.
[15] F. Nishino, M. Jeem, L. Zhang, K. Okamoto, S. Okabe, S. Watanabe, Formation of CuO nano-flowered surfaces via submerged photo-synthesis of crystallites and their antimicrobial activity, Scientific Reports, 7 (2017) 1063.
[16] M. Jeem, L. Zhang, J. Ishioka, T. Shibayama, T. Iwasaki, T. Kato, S. Watanabe, Tuning Optoelectrical Properties of ZnO Nanorods with Excitonic Defects via Submerged Illumination, Nano Letters, 17 (2017) 2088-2093.
[17] J. Ishioka, K. Kogure, K. Ofuji, K. Kawaguchi, M. Jeem, T. Kato, T. Shibayama, S. Watanabe, In situ direct observation of photocorrosion in ZnO crystals in ionic liquid using a laser-equipped high-voltage electron microscope, Aip Adv, 7 (2017) 035220.
[18] W. Wang, L. Xu, R. Zhang, J. Xu, F. Xian, J. Su, F. Yang, Coexistence of ferromagnetism and paramagnetism in ZnO/CuO nanocomposites, Chemical Physics Letters, (2019).
[19] M. Kumar, V. Bhatt, A. Kumar, J.-H. Yun, Nano lily-buds garden like ZnO nanostructures based gas sensor for H2 detection, Materials Letters, 240 (2019) 13-16.
[20] A. Ali, G. Rahman, T. Ali, M. Nadeem, S.K. Hasanain, M. Sultan, Enhanced band edge luminescence of ZnO nanorods after surface passivation with ZnS, Physica E: Low-dimensional Systems and Nanostructures, 103 (2018) 329-337.
[21] Y.H. Lu, M. Xu, L.X. Xu, C.L. Zhang, Q.P. Zhang, X.N. Xu, S. Xu, K. Ostrikov, Enhanced ultraviolet photocatalytic activity of Ag/ZnO nanoparticles synthesized by modified polymer-network gel method, Journal of Nanoparticle Research, 17 (2015) 350.
[22] R. Al-Gaashani, S. Radiman, A.R. Daud, N. Tabet, Y. Al-Douri, XPS and optical studies of different morphologies of ZnO nanostructures prepared by microwave methods, Ceramics International, 39 (2013) 2283-2292.
[23] M. Mouanga, M. Puiggali, B. Tribollet, V. Vivier, N. Pébère, O. Devos, Galvanic corrosion between zinc and carbon steel investigated by local electrochemical impedance spectroscopy, Electrochimica Acta, 88 (2013) 6-14.
[24] Z. Zheng, Z.S. Lim, Y. Peng, L. You, L. Chen, J. Wang, General Route to ZnO Nanorod Arrays on Conducting Substrates via Galvanic-cell-based approach, Scientific Reports, 3 (2013) 2434.
[25] E. Tada, K. Sugawara, H. Kaneko, Distribution of pH during galvanic corrosion of a Zn/steel couple, Electrochimica Acta, 49 (2004) 1019-1026.
[26] A. Goux, T. Pauporté, J. Chivot, D. Lincot, Temperature effects on ZnO electrodeposition, Electrochim. Acta, 50 (2005) 2239-2248.
[27] S. Le Caër, Water Radiolysis: Influence of Oxide Surfaces on H_2 Production under Ionizing Radiation, Water, 3 (2011) 235-253.

[28] J. Kim, W. Kim, K. Yong, CuO/ZnO Heterostructured Nanorods: Photochemical Synthesis and the Mechanism of H2S Gas Sensing, The Journal of Physical Chemistry C, 116 (2012) 15682-15691.
[29] W. Khan, S.-D. Kim, Ultra-violet photo-response characteristics of p-Si/i-SiO2/n-ZnO heterojunctions based on hydrothermal ZnO nanorods, Materials Science in Semiconductor Processing, 66 (2017) 232-240.
[30] P. Camarda, F. Messina, L. Vaccaro, S. Agnello, G. Buscarino, R. Schneider, R. Popescu, D. Gerthsen, R. Lorenzi, F.M. Gelardi, M. Cannas, Luminescence mechanisms of defective ZnO nanoparticles, Physical Chemistry Chemical Physics, 18 (2016) 16237-16244.
[31] B.K. Sharma, N. Khare, D. Haranath, Photoluminescence lifetime of Al-doped ZnO films in visible region, Solid State Communications, 150 (2010) 2341-2345.
[32] S.K. Mishra, S. Srivastava, R.K. Srivastava, A.C. Panday, S.G. Prakash, Photoluminescence and ultraviolet photoresponse in ZnO nanophorsphors prepared by thermal decomposition of zinc acetate, Adv. Mater. Lett., 2 (2011) 298-302.
[33] M. Wang, L. Jiang, E. Kim, S. Hong Hahn, Electronic structure and optical properties of Zn(OH) 2 : LDA+U calculations and intense yellow luminescence, 2015.
[34] O. Schmidt, A. Geis, P. Kiesel, C.G. Van de Walle, N.M. Johnson, A. Bakin, A. Waag, G.H. Döhler, Analysis of a conducting channel at the native zinc oxide surface, Superlattices Microstruct., 39 (2006) 8-16.
[35] Z. Fan, D. Wang, P.-C. Chang, W.-Y. Tseng, J.G. Lu, ZnO nanowire field-effect transistor and oxygen sensing property, Appl. Phys. Lett., 85 (2004) 5923-5925.

Figure captions

Fig. 1. Schematic setup of G-SPSC experiment. (a) Galvanic contact setup between Zn-Cu plates. (b) G-SPSC experiment inside a dark chamber. (c) One-dimensional ZnO@Cu NRs growth on red circle-marked sample area after G-SPSC.

Fig. 2. (a) Illustration for galvanic contact setup between a Zn wire and Cu plate. (b-c) FE-SEM images of ZnO@Cu NRs after UV irradiation of 24 h and 48 h, respectively. The right panel is magnified image of marked area. (d) Typical XRD spectrum of ZnO@Cu NRs. (e-f) FE-SEM images of ZnO@Cu NRs after UV irradiation with and without galvanic contact, respectively. Inset schematics are the Zn-Cu plates arrangement during G-SPSC experiment.

Fig. 3. (a) Representative TEM image of pencil-like shape ZnO NR. (b) SAED pattern of the NR obtained along $[1\bar{1}0]$ direction. (c) HRTEM image of the NR and (d) and its magnified inversed Fourier transformed image, obtained from the yellow marked area.

Fig. 4. XPS spectra of ZnO@Cu NRs. (a) Representative wide scan survey spectrum. (b) Zn 2p state the NRs. (c-d) XPS spectra of the NRs O 1s state after UV 24h and UV 48h irradiation, respectively.

Fig. 5. ZnO@Cu NRs growth mechanism under G-SPSC.

Fig. 6. Qualitative pH change measurement on Zn-Cu plates with (a) prepared BTB agar solution. (b) Initial green color of BTB transformation to yellow and blue denoting acidic and alkaline pH, respectively. (c) Photographs of 24 h G-SPSC treated Zn-Cu plates inside BTB agar solution. Gradient of blue color evolved at the margin of samples, exhibiting alkaline biased reaction.

Fig. 7. Room-temperature PL spectra of ZnO@Cu NRs after UV 24h (blue line) and UV 48 h (red line). (a) Comparison of 24h sample and 48h sample. (b-c) Gaussian deconvolution results on PL spectra of (b) UV 24h and (c) UV 48h G-SPSC samples.

Table 1. Peak deconvolution result for O 1*s* spectra.

Table 2. Peak assignment in PL spectra of ZnO@Cu NRs.

Fig. S1. G-SPSC effect on NRs growth (a) with and (b) without UV irradiation.

Fig. S1 depicts the feasibility of NRs growth in G-SPSC experiment with and without UV irradiation.

In the experiment, both setups include Cu plate wrapped with Zn wire. Then, the sample was immersed in deaerated distilled water contained by cuvette cells. Both cells were placed together under 24h UV irradiation in a dark chamber, with (b) cell was shielded by aluminum foil to prevent UV light but maintain the water temperature increase. Metallic luster of Zn wire was decreased according to the taken optical photographs and white layer formed near the wire. The white layer generously spread at the bottom area of Cu plate, built by the ZnO NRs as revealed by SEM observation. Instead of white, dark layer was observed on the same area of (b) sample, which contain very less ZnO NRs and dominantly covered by $Zn(OH)_2$. OH^- production was suppressed without light-induced water splitting as described by Fig. 5, which inhibit the transformation of $Zn(OH)_2$ species to ZnO.

Galvanic-Submerged Photo Synthesis of Crystallites: Fabrication of ZnO nanorods @ Cu-surface

ALL FIGURES

Yuki Takahashi, Kento Hiraiwa, Melbert Jeem, Lihua Zhang, and Seiichi Watanabe

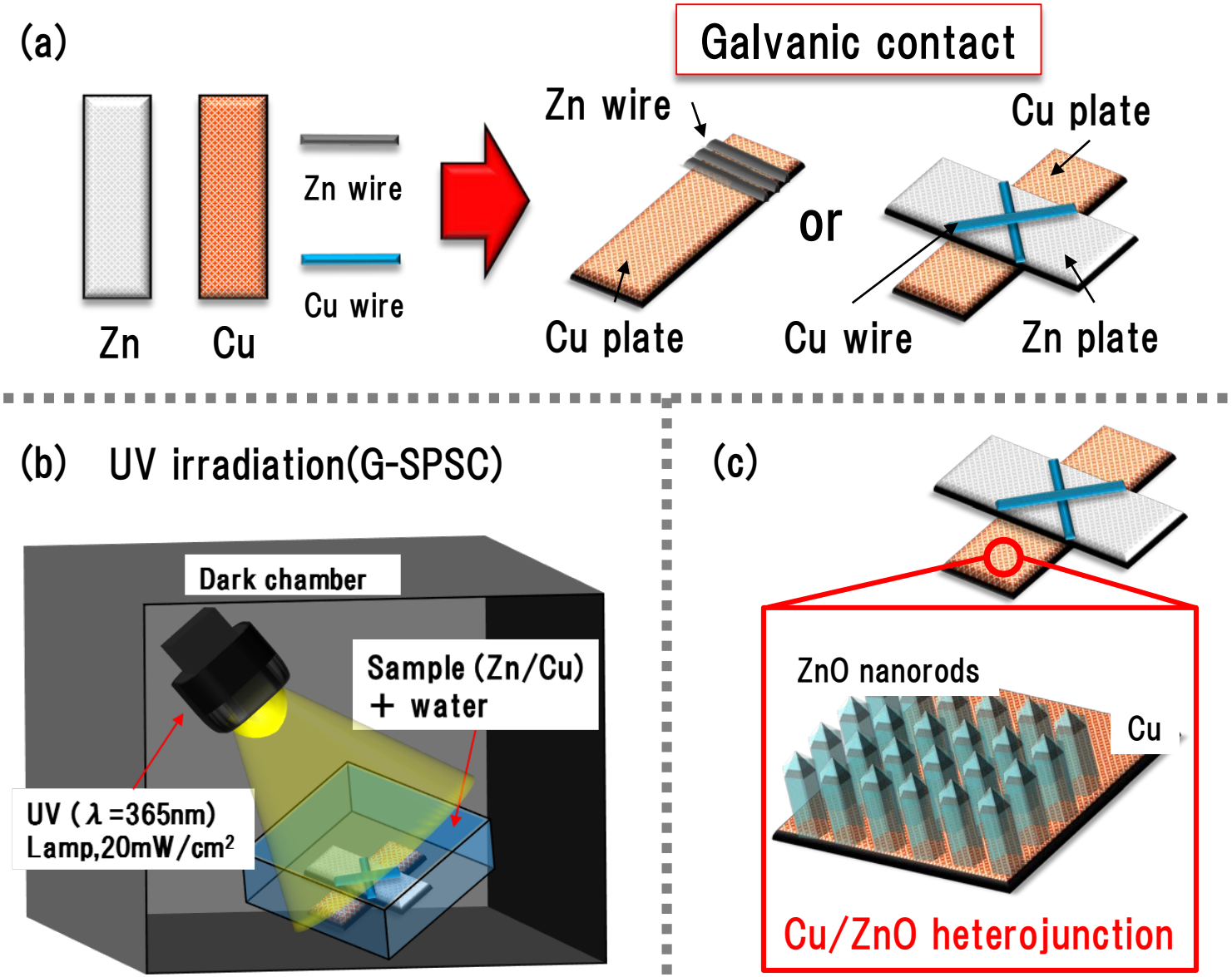

Fig. 1. Schematic setup of G-SPSC experiment. (a) Galvanic contact setup between Zn-Cu plates. (b) G-SPSC experiment inside a dark chamber. (c) One-dimensional ZnO@Cu NRs growth on red circle-marked sample area after G-SPSC.

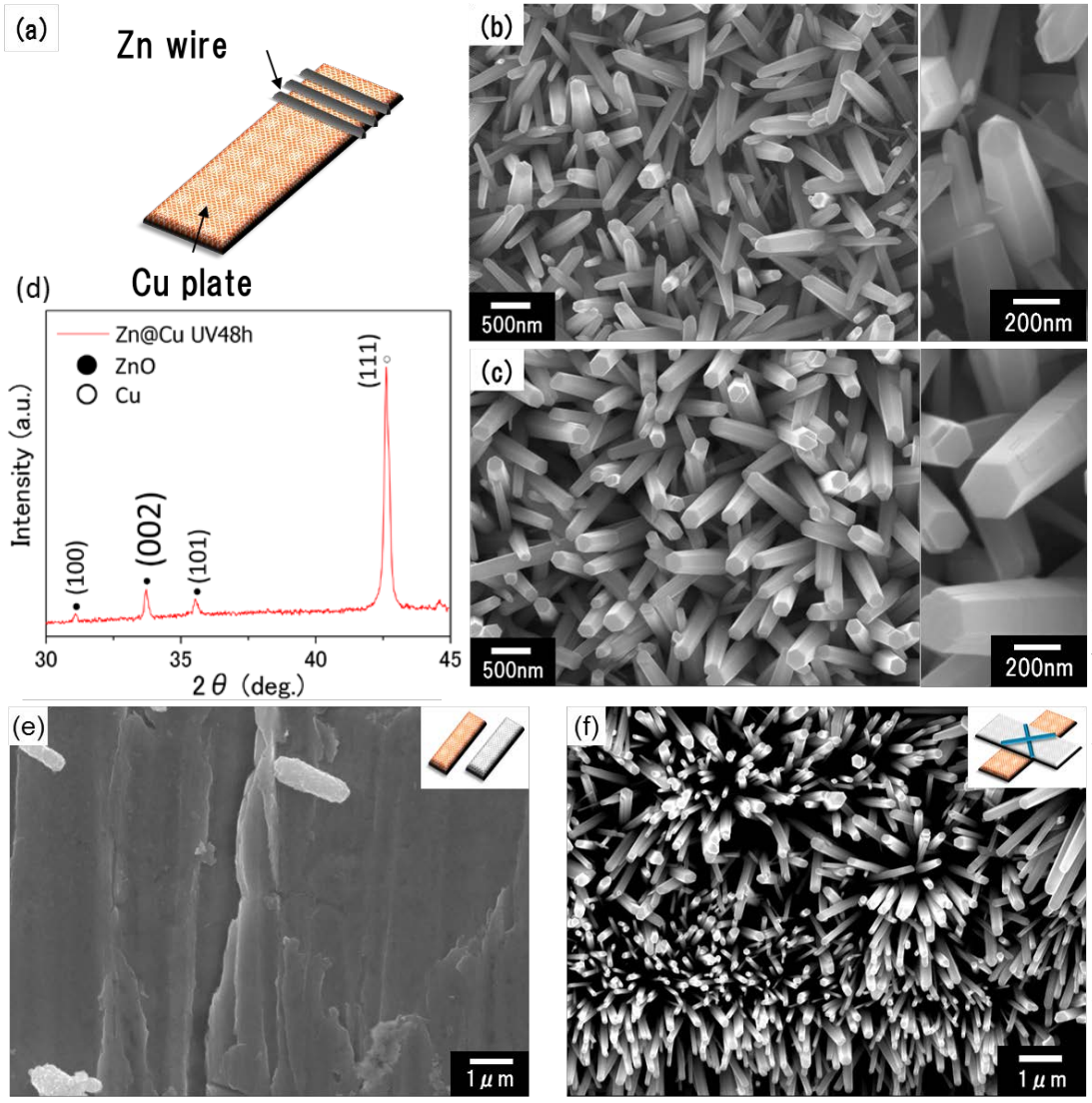

Fig. 2. (a) Illustration for galvanic contact setup between a Zn wire and Cu plate. (b-c) FE-SEM images of ZnO@Cu NRs after UV irradiation of 24 h and 48 h, respectively. The right panel is magnified image of marked area. (d) Typical XRD spectrum of ZnO@Cu NRs. (e-f) FE-SEM images of ZnO@Cu NRs after UV irradiation with and without galvanic contact, respectively. Inset schematics are the Zn-Cu plates arrangement during G-SPSC experiment.

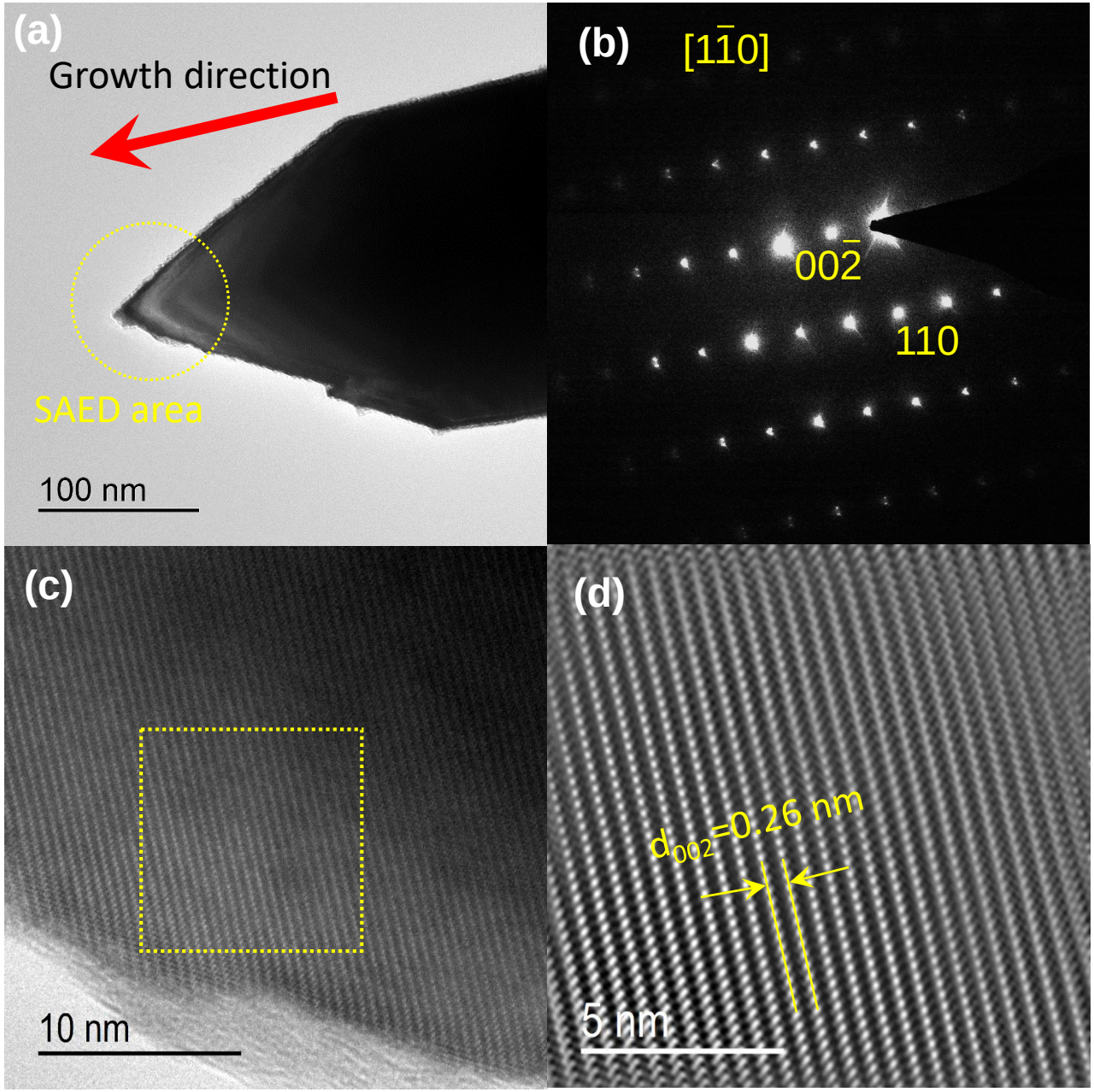

Fig. 3. (a) Representative TEM image of pencil-like shape ZnO NR. (b) SAED pattern of the NR obtained along [1$\bar{1}$0] direction. (c) HRTEM image of the NR and (d) its magnified inversed Fourier transformed image, obtained from the yellow marked area.

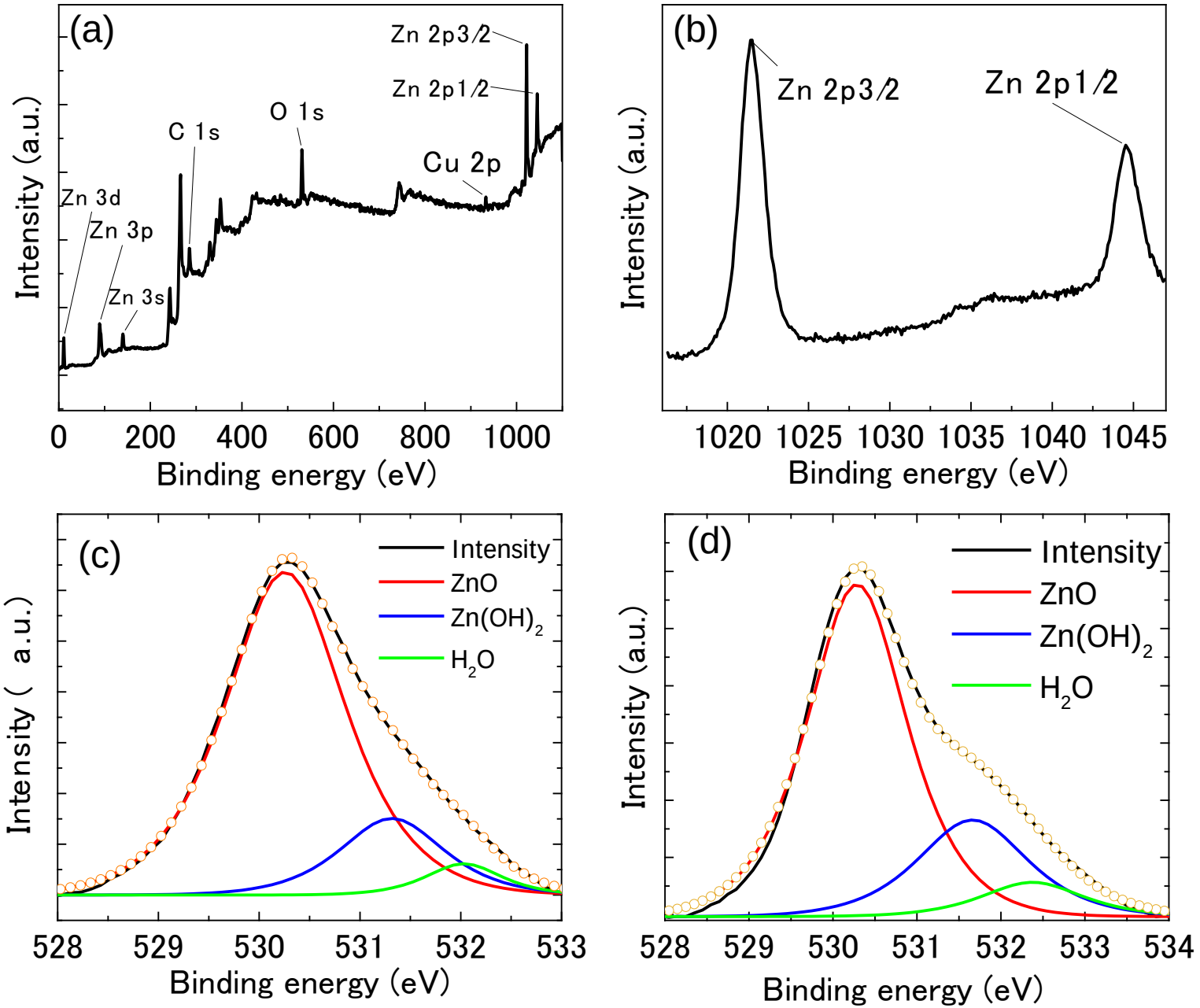

Fig. 4. XPS spectra of ZnO@Cu NRs. (a) Representative wide scan survey spectrum. (b) Zn 2*p* state of the NRs. (c-d) XPS spectra of the NRs O 1*s* state after UV 24h and UV 48h irradiation, respectively.

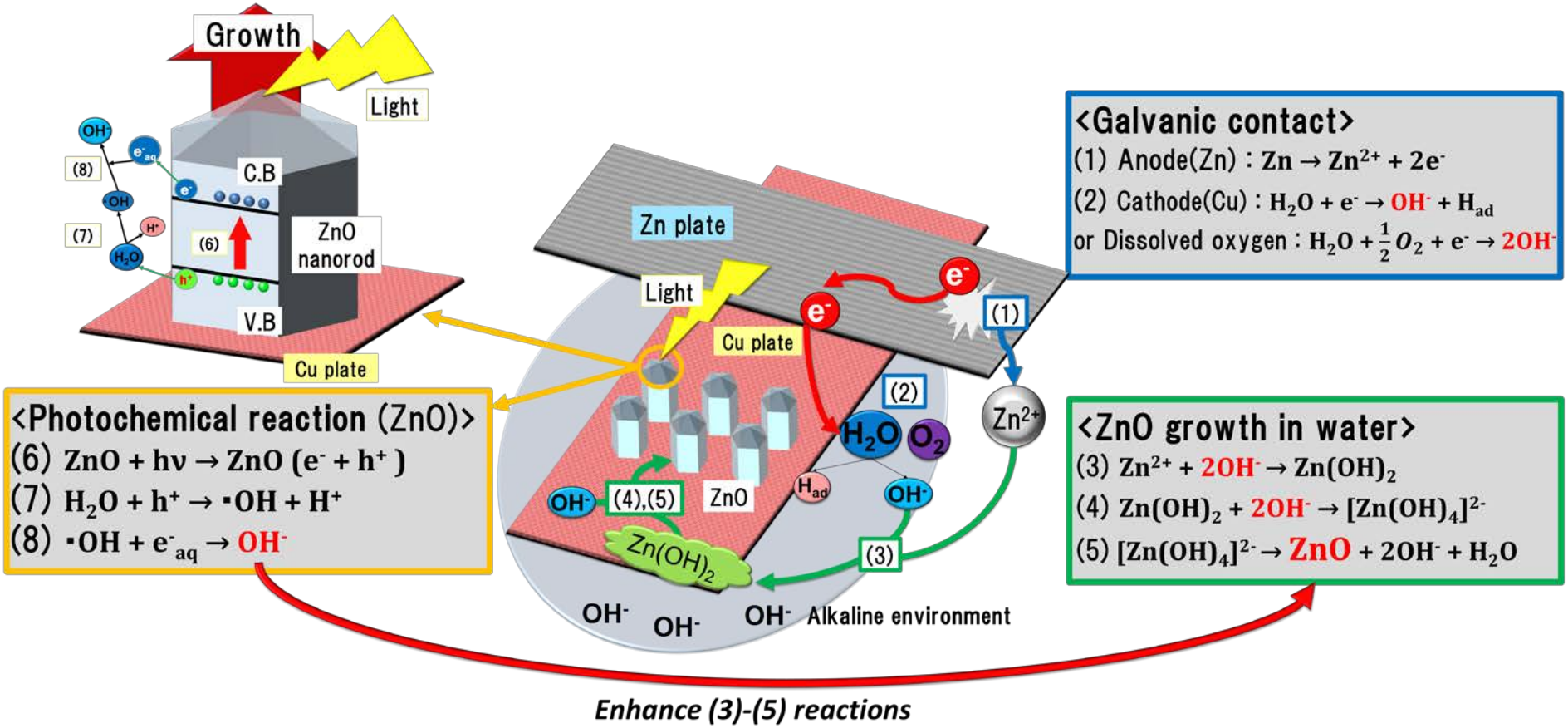

Fig. 5. ZnO@Cu NRs growth mechanism under G-SPSC.

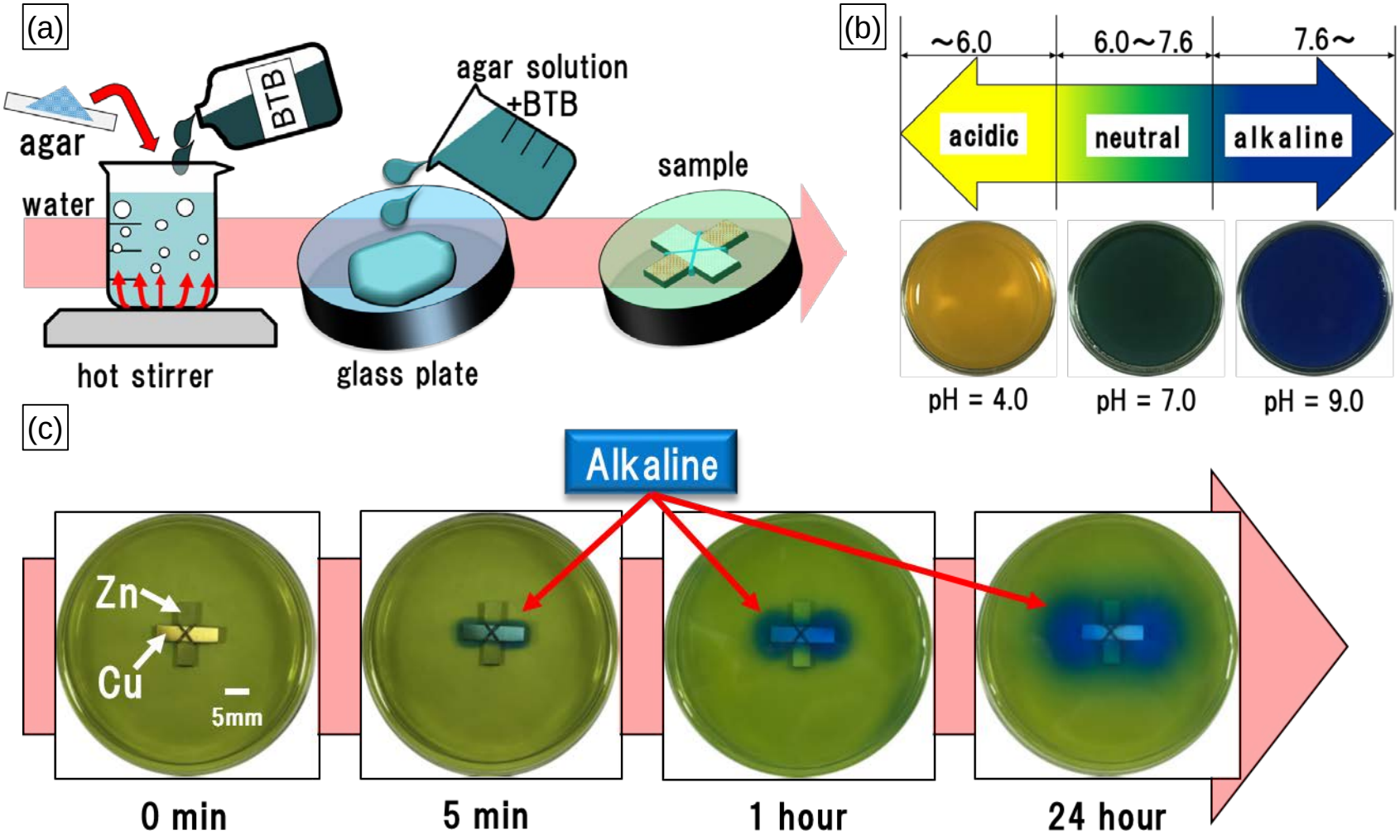

Fig. 6. Qualitative pH change measurement on Zn-Cu plates with (a) prepared BTB agar solution. (b) Initial green color of BTB transformation to yellow and blue denoting acidic and alkaline pH, respectively. (c) Photographs of 24 h G-SPSC treated Zn-Cu plates inside BTB agar solution. Gradient of blue color evolved at the margin of samples, exhibiting alkaline biased reaction.

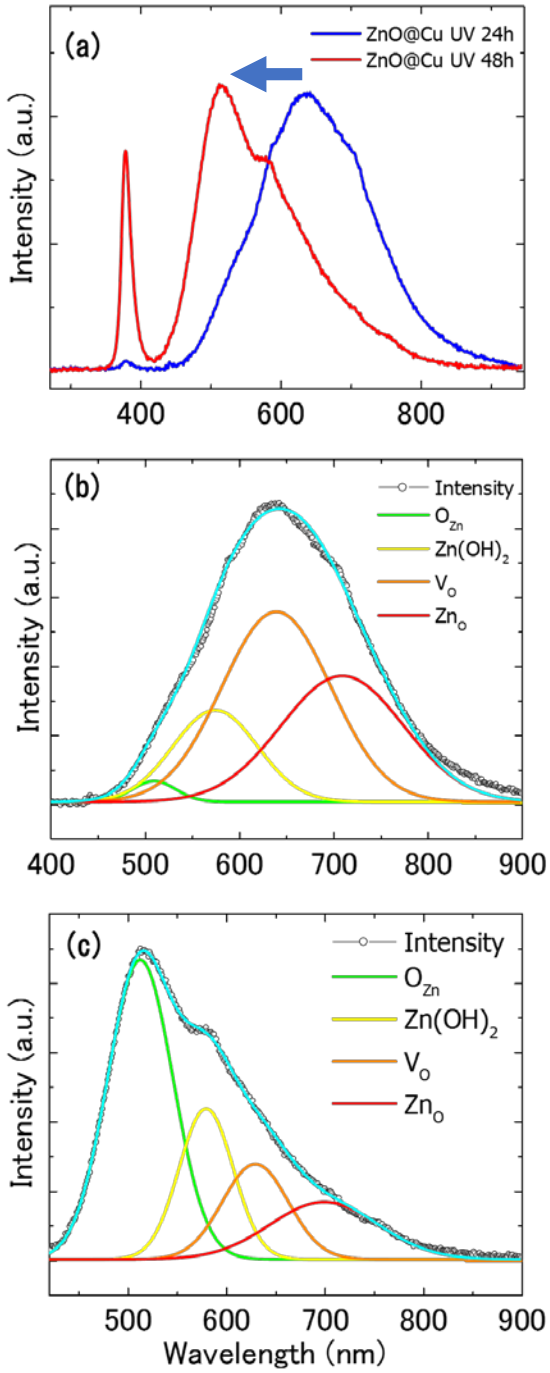

Fig. 7. Room-temperature PL spectra of ZnO@Cu NRs after UV 24h (blue line) and UV 48 h (red line). (a) Comparison of 24h sample and 48h sample. (b-c) Gaussian deconvolution results on PL spectra of (b) UV 24h and (c) UV 48h G-SPSC samples.

Table 1. Peak deconvolution result for O 1*s* spectra.

	ZnO	$Zn(OH)_2$	H_2O
ZnO/Cu UV24h	530.3	531.3	532.0
ZnO/Cu UV48h	530.3	531.6	532.3

Table 2. Peak assignment in PL spectra of ZnO@Cu NRs.

Wavelength (nm)	510 – 520	570 – 580	630 – 640	700 -710
Peak assignment	O_{Zn}	$Zn(OH)_2$	V_O	Zn_O

Galvanic-Submerged Photo Synthesis of Crystallites: Fabrication of ZnO nanorods @ Cu-surface

SUPPLEMENTARY MATERIALS

Yuki Takahashi, Kento Hiraiwa, Melbert Jeem, Lihua Zhang, and Seiichi Watanabe

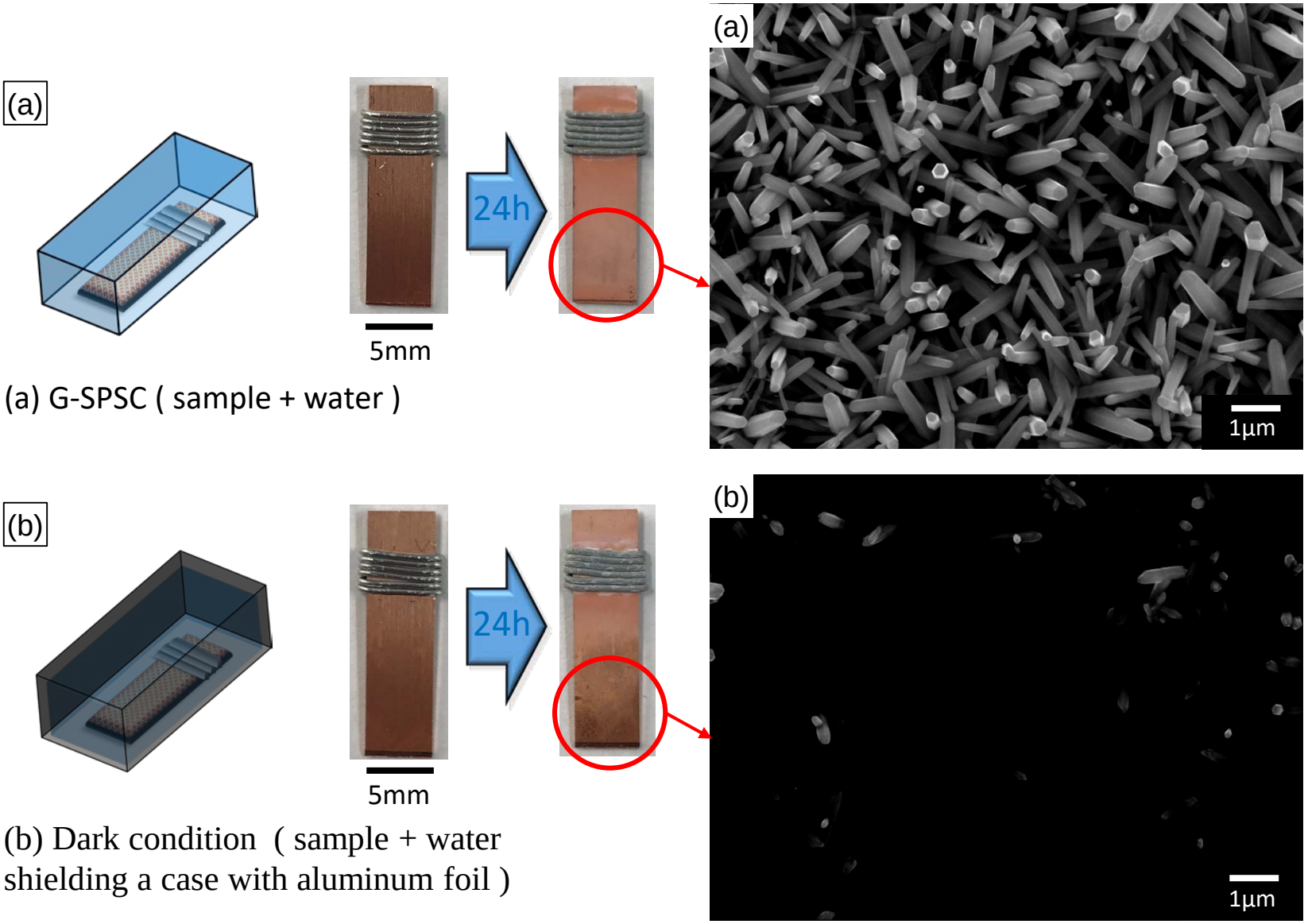

Fig. S1 G-SPSC effect on ZnO NRs growth (a) with and (b) without UV irradiation.

Fig. S1 depicts the feasibility of NRs growth in G-SPSC experiment with and without UV irradiation. In the experiment, both setups include Cu plate wrapped with Zn wire. Then, the sample was immersed in deaerated distilled water contained by cuvette cells. Both cells were placed together under 24h UV irradiation in a dark chamber, with (b) cell was shielded by aluminum foil to prevent UV light but maintain the water temperature increase. Metallic luster of Zn wire was decreased according to the taken optical photographs and white layer formed near the wire. The white layer generously spread at the bottom area of Cu plate, built by the ZnO NRs as revealed by SEM observation. Instead of white, dark layer was observed on the same area of (b) sample, which contain very less ZnO NRs and dominantly covered by $Zn(OH)_2$. OH^- production was suppressed without light-induced water splitting as described by Fig. 5, which inhibit the transformation of $Zn(OH)_2$ species to ZnO.

RAW FIGURES & DATA

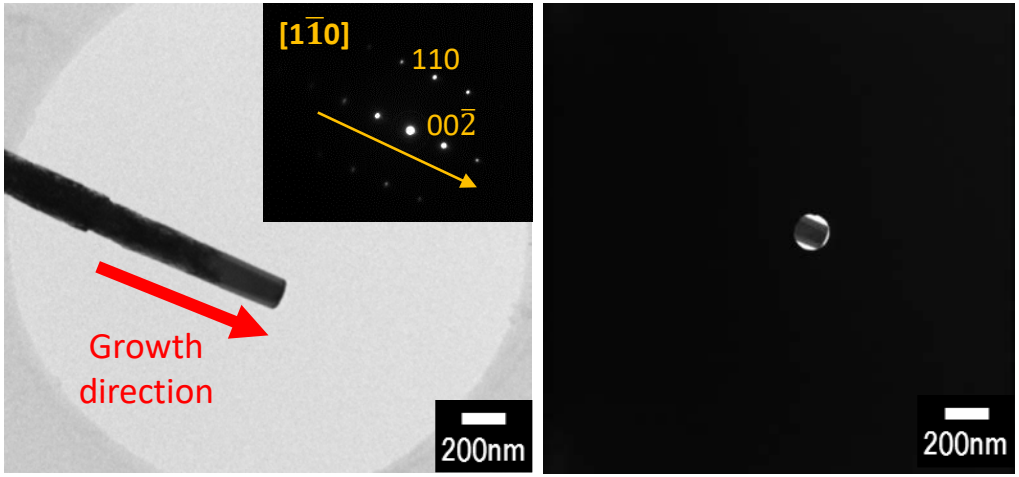
[1$\bar{1}$0]
110
00$\bar{2}$
Growth
direction
200nm
200nm

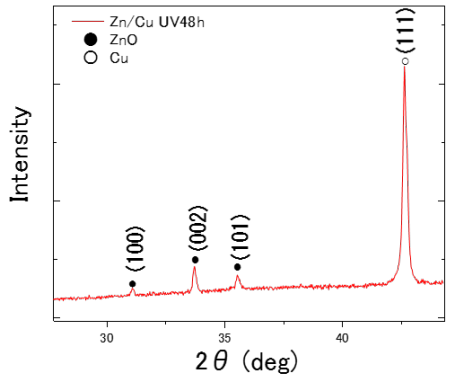
Zn/Cu UV48h
ZnO
Cu
(111)
(100)
(002)
(101)
Intensity
30
35
40
2θ (deg)

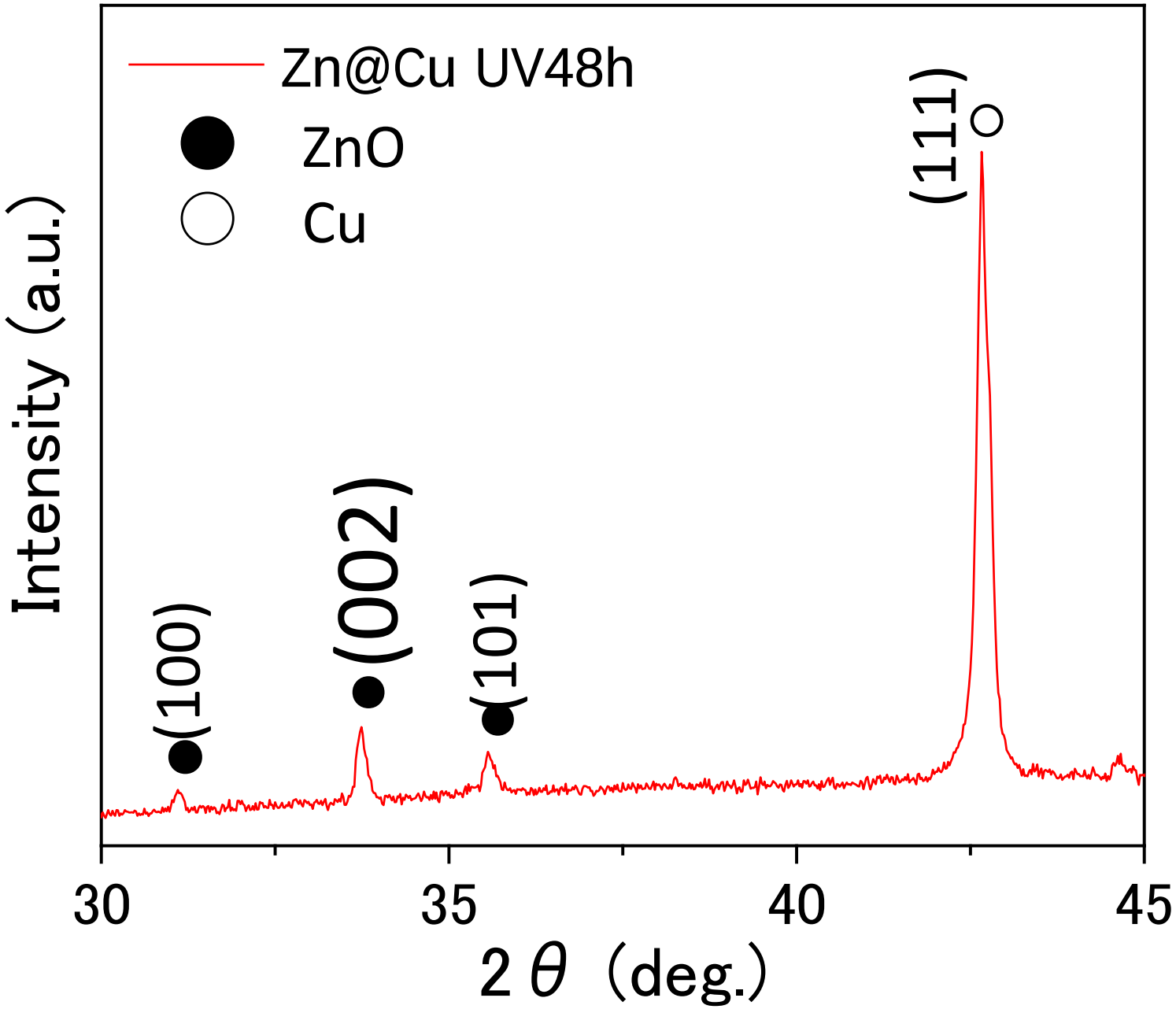
Zn@Cu UV48h
ZnO
Cu
(100)
(002)
(101)
(111)
Intensity (a.u.)
30
35
40
45
2θ (deg.)

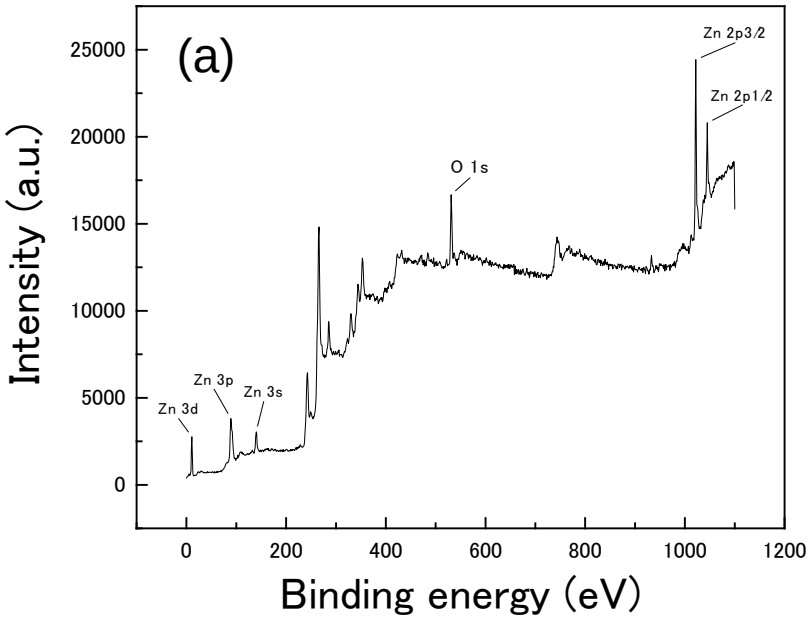
(a)
Intensity (a.u.)
Binding energy (eV)
Zn 3d
Zn 3p
Zn 3s
O 1s
Zn 2p3/2
Zn 2p1/2
0
5000
10000
15000
20000
25000
0
200
400
600
800
1000
1200

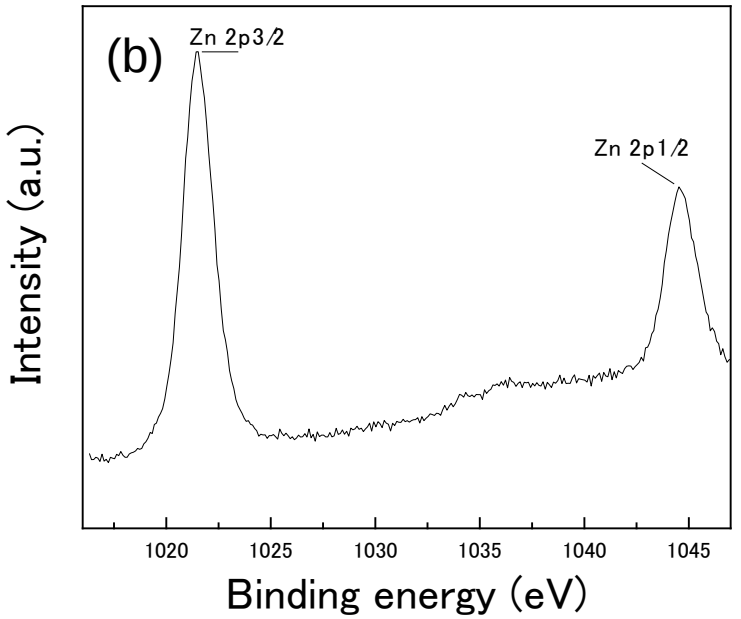
(b)
Intensity (a.u.)
Binding energy (eV)
Zn 2p3/2
Zn 2p1/2
1020
1025
1030
1035
1040
1045

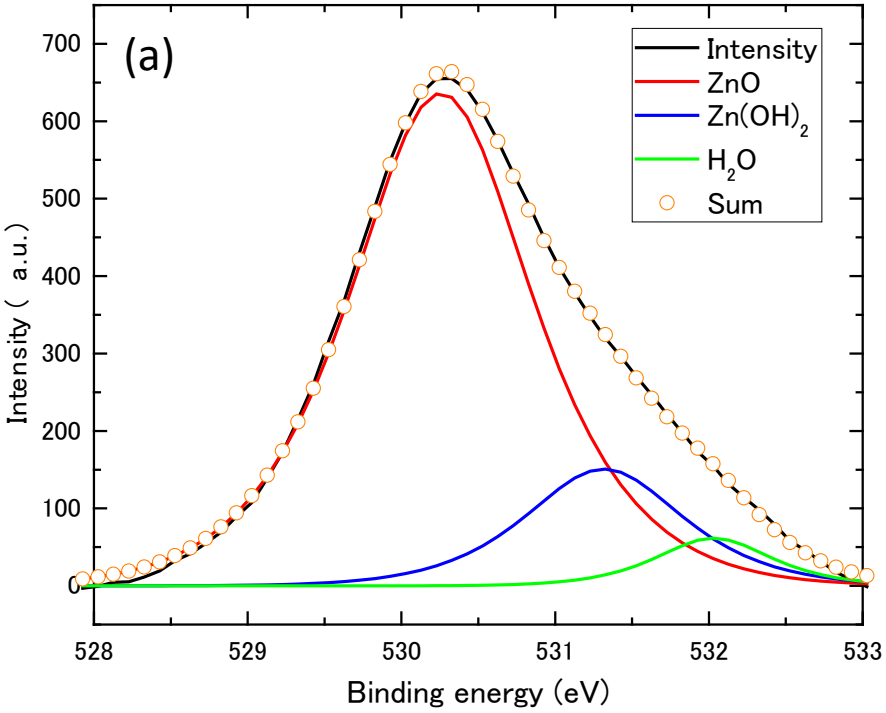

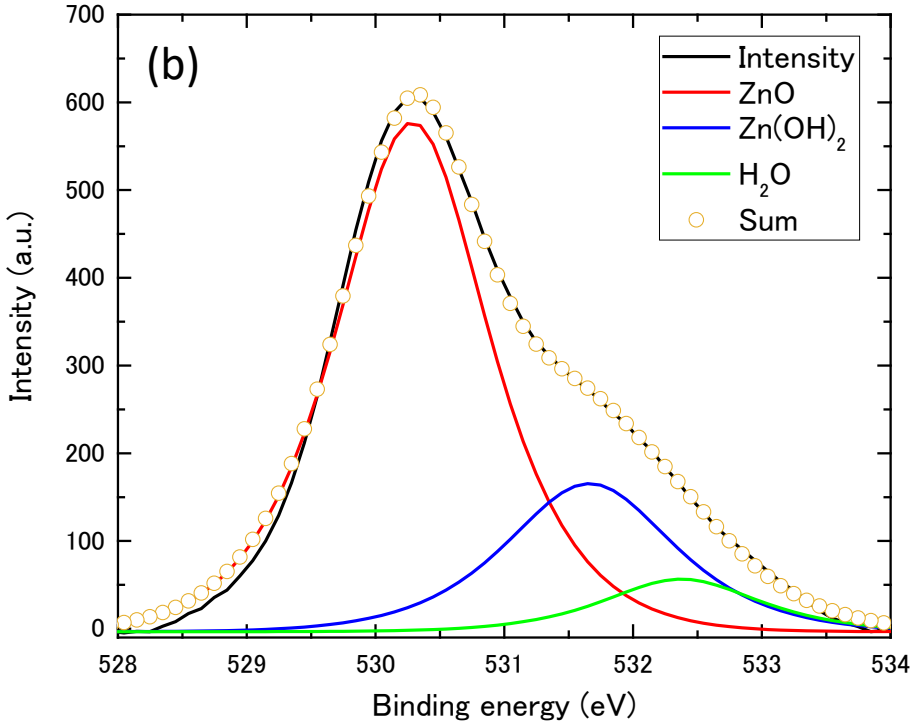

	O	Zn
(a) 24h UV irradiation	48.4	51.6
(b) 48h UV irradiation	54.8	45.2

Fig. 6 ?
??

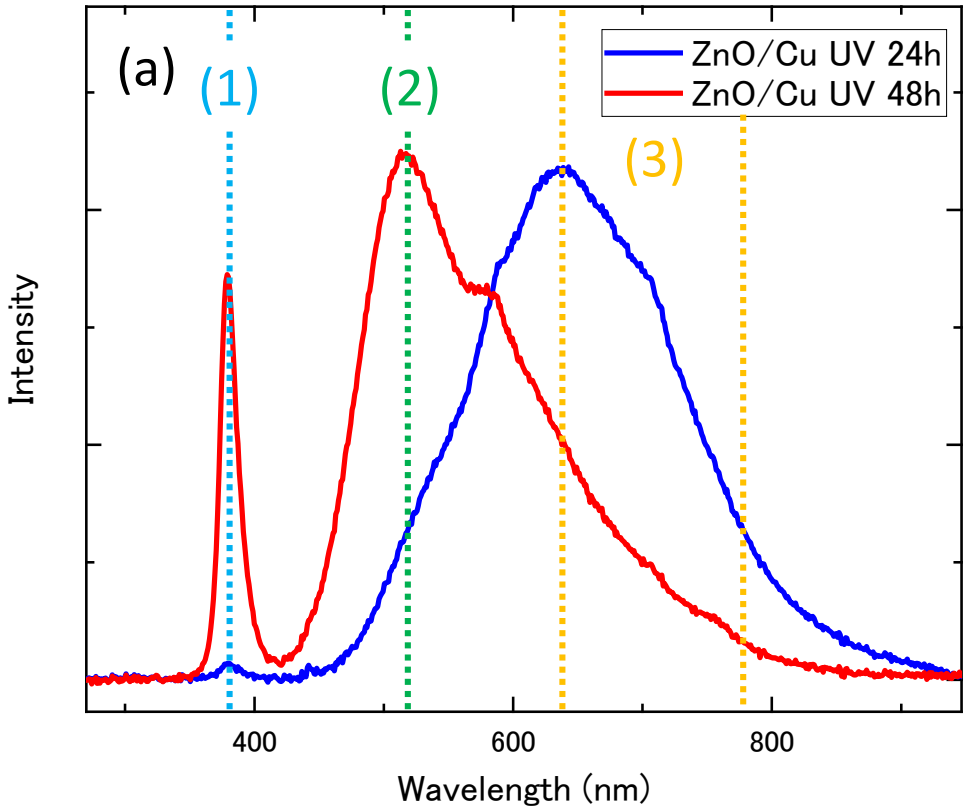
(a)
(1)
(2)
(3)
ZnO/Cu UV 24h
ZnO/Cu UV 48h
Intensity
400
600
800
Wavelength (nm)

24h peak analysis

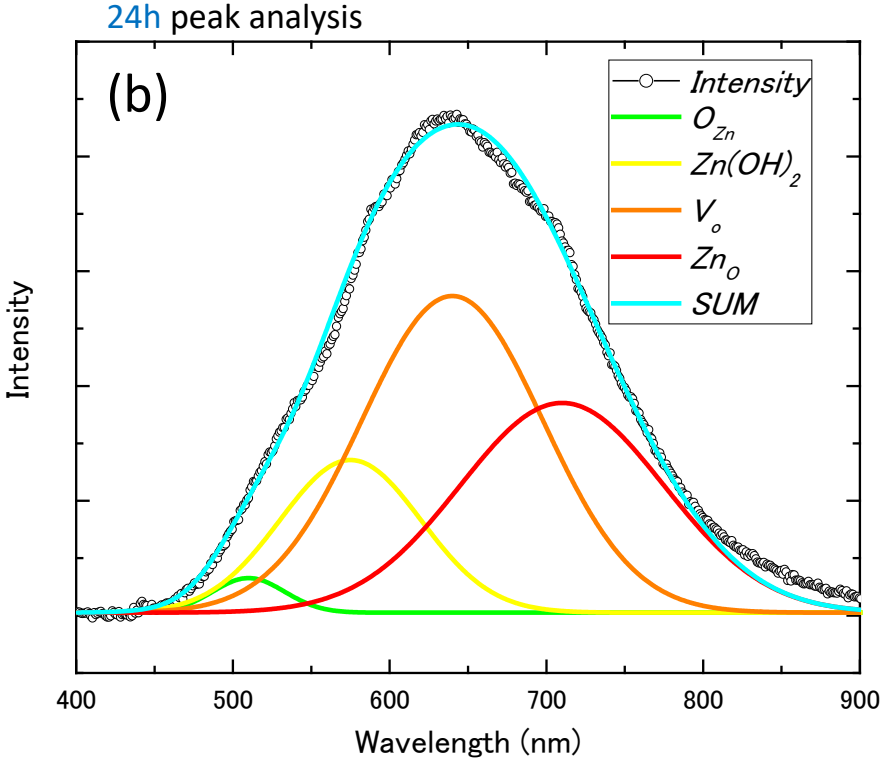

48h peak analysis